An experimental and theoretical study of the reaction of ethynyl radicals with nitrogen dioxide (HC ≡ C + NO 2)

Shaun A. Carl, Hue Minh Thi Nguyen, Minh Tho Nguyen, and Jozef Peeters

Citation: The Journal of Chemical Physics **118**, 10996 (2003); doi: 10.1063/1.1573192
View online: http://dx.doi.org/10.1063/1.1573192
View Table of Contents: http://scitation.aip.org/content/aip/journal/jcp/118/24?ver=pdfcov
Published by the AIP Publishing

An experimental and theoretical study of the reaction of ethynyl radicals with nitrogen dioxide ($HC{\equiv}C+NO_2$)

Shaun A. Carl,[a] Hue Minh Thi Nguyen,[b] Minh Tho Nguyen, and Jozef Peeters
Department of Chemistry, University of Leuven, Celestijnenlaan 200F, B-3001 Leuven, Belgium

(Received 10 February 2003; accepted 18 March 2003)

A pulsed laser photolysis/chemiluminescence (PLP/CL) technique was used to determine absolute rate constants of the reaction $C_2H+NO_2\rightarrow$products over the temperature range 288–800 K at a pressure of 5 Torr (N_2). The reaction has a large rate constant that decreases with increasing temperature. It may be expressed in simple Arrhenius form as $k_1(T)=(7.6\pm1.0)\times10^{-11}\exp[(130\pm50)\ \mathrm{K}/T]$, although there is an indication of a downward curvature for $T>700$ K. A three-parameter Arrhenius fit to the data, which takes this into account gives $k_1(T)=(9.7\pm1.5)\times10^{-9}T^{-0.68}\exp[(158\pm65)\ \mathrm{K}/T]$. Our experiments also show that the 293 K rate constant is invariant to pressure between 2 and 11 Torr (N_2). We have also characterized the C_2H+NO_2 reaction theoretically. A large portion of the potential energy surface (PES) of the [C_2,H,N,O_2] system has been investigated in its electronic (singlet) ground-state using DFT with the B3LYP/6-311++G($3df$,$2p$) method and MO computations at the CCSD(T)/6-311++G(d,p) level of theory. Seventeen isomers and thirty-two transition structures were found to connect reactants to products following eighteen different channels. Hydroxyl cyano ketone **11** and formylisocyanate **16** were found to be the most stable intermediates, although the reaction flux through them, as a fraction of the total, is likely to be small over the temperature range studied. A part of the PES corresponds with that of the HCCO+NO reaction [I. V. Tokmakov, L. V. Moskaleva, D. V. Paschenko, and M. C. Lin, J. Phys. Chem. A **167**, 1066 (2003)], and the dominant product channels for C_2H+NO_2 proceed via the same nitrosoketene intermediate that is formed initially in the HCCO+NO reaction. However, unlike in the latter reaction, the fate of the much more highly excited nitrosoketene formed by C_2H+NO_2 is likely to be governed dynamically. We present arguments as to the likely product channels for C_2H+NO_2 based on both statistical and dynamical considerations. A statistical description overwhelmingly favors the product set HCCO+NO. Dynamical considerations on the other hand favor both the HCN+CO_2 and HCCO+NO product sets. Formation of HCNO+CO appears unlikely. Energetically allowed paths, leading to five other product sets, namely, HNCO+CO, HOCN+CO, HOCC+NO, HONC+CO, and HNC+CO_2, have also been identified, and are discussed. © *2003 American Institute of Physics.* [DOI: 10.1063/1.1573192]

I. INTRODUCTION

The ethynyl radical (C_2H) has been detected in interstellar space[1–4] and in planetary atmospheres.[5,6] Thus its low-temperature kinetics have received a great deal of attention in recent years.[7–12] It is also known to play a major role in the high-temperature chemistry of combustion,[13,14] where it is linked to the ubiquitous acetylene oxidation reaction that leads, via the highly reactive $CH_2(\tilde{a}\,^1A_1)$ and $CH(X\,^2\Pi)$ radicals, to C_3H_x ($x=0-4$).[15] From this C_3H_x backbone, the different species within which are connected by reactions of H_2 and H, a number of routes have also been proposed for formation of the first aromatic ring structures.[16–19] These are the building blocks of polycyclic aromatic hydrocarbons (PAH), which are the likely precursors of soot particles in aliphatic hydrocarbon fuel combustion.

Besides C_2H formation in flames by H-atom abstraction reactions of C_2H_2 with H, OH, or O, other routes have been proposed in which C_2H is formed by O or OH reactions with a C_3H_x ($x=0$ to 3) species; more specifically C_2H was shown to be formed by C_3H_2+O in C_2H_2/H/O atomic flames.[20] Further reaction of C_2H with C_2H_2 leads to the C_4H_n ($2\leqslant n\leqslant5$) series[14,21,22] and by reaction of C_2H_2 with C_4H_3 or C_4H_5 the aromatics C_6H_5 or C_6H_6, respectively, are formed.

In order to refine our knowledge of the complex chemistry of small hydrocarbon radicals in combustion environments we have recently studied the kinetics of the reactions of C_2H with O_2, C_2H_2, H_2, NO, CH_4, and C_2H_6 over an extended temperature range.[23–31] We have also unambiguously identified the reactions of C_2H with O atoms as the dominant source of $CH(A\,^2\Delta)$ chemiluminescence in C_2H_2/O/H atomic flames,[32] and in a separate study we have shown that the $CH(A\,^2\Delta)$ yield of the very fast $C_2H+O\rightarrow CH+CO$ reaction[33] is of the order of 8%.[34]

As with PAH and soot formation, reactions of the oxides

[a]Author to whom correspondence should be addressed. Electronic mail: Shaun.Carl@chem.kuleuven.ac.be
[b]On leave from Faculty of Chemistry, University of Education, Hanoi, Vietnam.

of nitrogen NO_x in combustion environments have continued to attract the attention of experimental as well as theoretical scientists due to their detrimental implications for our atmospheric environment. This has led to the development of techniques to reduce NO_x emissions such as thermal $DeNO_x$,[35] NO_x-OUT,[36] $RAPRENO_x$,[37] and NO-reburning,[38–40] the underlying chemistry of which is still not adequately characterized.[41] We have contributed to improving our understanding of this complex NO_x chemistry by investigating reactions such as C_2H+NO,[28,24] $NO+C_2H_2$,[42] $NO+C_2H_3$,[43] and $HCCO+NO$.[44,45] Rate constants for the reaction C_2H+NO_2 represent significant missing data in NO_x chemistry at combustion temperatures. We have thus focused our attention on this reaction in the present work.

In stationary source hydrocarbon combustion, a large fraction of NO_x is in the form of NO so that reactions of small hydrocarbon radicals with this species usually dominate their NO_2 counterparts, particularly at high temperatures. The degree of participation of NO_2 in NO_x flame chemistry depends largely on the temperature-sensitive $[NO_2] \Leftrightarrow [NO]$ quasi-steady-state, which is controlled mainly by the reactions $NO+HO_2 \rightarrow NO_2+OH$, $NO_2+H \rightarrow NO+OH$, $NO+H+M \rightarrow HNO+M$, and $HNO+H \rightarrow NO+H_2$. They usually dictate that concentrations of NO_2 are significant at temperatures below about 1500 K. Thus in low-temperature and fuel-rich regions—those found in typical NO-reburning conditions, for example—radical reactions involving NO_2 are expected to be significant.

Further, the C_2H radical is one of only a few radicals that is amenable to detection in combustion systems by chemiluminescence emissions [via C_2H+O (and O_2) $\rightarrow CH(A\,^2\Delta)+$prod.].[46,47] Thus in order to make full use of these easily-detectable chemiluminescence signatures and to quantitatively relate them to the immediate chemical environment it is necessary to characterize fully the reactivity of the precursor species, viz., C_2H, of the characteristic blue, $CH(A) \rightarrow (X)$, emissions.

Of particular relevance to the present investigation are the experimental and theoretical product distribution studies of the reaction $HCCO+NO$ since part of the PES is common to that of the C_2H+NO_2 reaction. Experimental investigations of the product branching for the $HCCO+NO$ reaction of Boullart *et al.*,[48] Rim and Hershberger,[49] and Eickhoff and Temps[50] show that the important reaction products are $(HCNO)_{isomer}+CO$ and $(HCN)_{isomer}+CO_2$, the former being dominant. In our earlier theoretical work[51] on the $HCCO+NO$ PES we have found that, besides the products $HCNO+CO$ and $HCN+CO_2$, a three-membered cyclic structure and formyl isocyanate (structures **14** and **16** of this work) are also stable isomers, but their connections with the reactants were not clear. In a subsequent publication,[52] we have presented an improved treatment of the PES using higher levels of theory and also performed RRKM-master equation analyses incorporating the effect of internal rotations on the state densities. Again only the two previously reported product channels[51] were found to be important, and $(HCNO)_{isomer}+CO$, was shown to be the dominant product, in agreement with direct experimental product data.[48–50]

The purpose of the present work is twofold. Firstly to determine experimentally the absolute rate constants for the reaction of C_2H with NO_2 for which no experimental data exists. Secondly, to explore the PES in great detail and to ascertain the likely products.

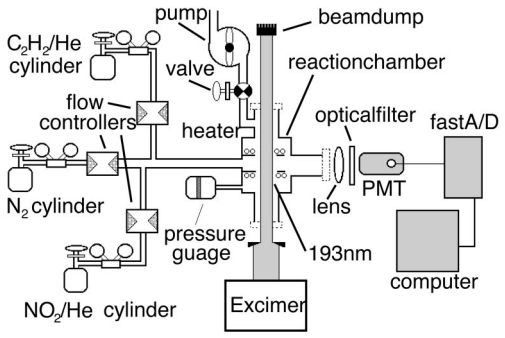

FIG. 1. Experimental pulsed photolysis/chemiluminescence apparatus used to determine absolute rate constants of the reaction $C_2H+NO_2 \rightarrow$ products.

II. EXPERIMENT

A. Apparatus and method

The pulsed-laser photolysis/chemiluminescence experimental apparatus (Fig. 1) used here to determine the absolute rate constants of C_2H+NO_2 is described in detail elsewhere.[53] Here we give a general outline with details specific to the present experiments.

C_2H radicals were generated in a small volume along the central axis and away from the walls of a stainless steel reaction chamber by pulsed laser photolysis of C_2H_2 at 193 nm (ArF excimer laser; $\approx$15 mJ cm^{-2} pulse^{-1}; 15 ns pulse^{-1}; 2 Hz repetition rate). The reaction cell was equipped with three quartz windows; two for passage of the photolysis beam through its center and one for UV-Vis detection at right angles to the photolysis beam's optical axis. The cell is connected to a vacuum/gas-flow system and a rotary vacuum pump allowing a continuous through-flow of gas mixtures of known homogeneous composition and constant total pressure (typically 5.0 Torr N_2, $\approx$666 Pa). All gases were obtained commercially and, with the exception of C_2H_2, used without further purification. The purities were as follows: N_2, 99.9997%, acting as a buffer; C_2H_2, 99.6% (UCAR); NO_2, 2.5% in ultrahigh purity He (Air Products). A further verification of the NO_2 fraction was performed in the laboratory using long-path visible absorption. A fraction, $[NO_2]/[\text{Total}]$, of $(2.47\pm0.06)\times10^{-2}$ was determined, in agreement with that stated by the manufacturer. Any acetone contained in the C_2H_2 sample was removed by trapping at 195 K. The gas mixtures in the reaction chamber were able to be heated to about 900 K by means of Ni/Cr resistive wire coils surrounding a ceramic tube (99.7% Al_2O_3, with an internal, gray, oxidized SiC coating) through which the gas mixtures flow. Temporal and spatial variations in the gas temperature during the experiments ranged from ±1 K at 288 K to ±15 K at 800 K, our highest-temperature experiment.

Concentrations of the co-reactant, $[NO_2]$, were accurately determined using total reactor pressure—measured by

a 10 Torr Barocel pressure sensor (Datametrics)—and partial flow rates—measured by calibrated mass flow controllers (MKS Instruments Inc.). Typical total flow rates through the reaction chamber were 200 sccm ($cm^3\,min^{-1}$ at STP); sufficiently high to remove reaction products between successive laser shots. Optical emissions from the center of the reaction chamber (see below) were imaged onto a optically-filtered photomultiplier tube (PMT). The resulting voltage was digitized by a fast 8-bit analog-to-digital converter (ADC 200, Pico Technology Ltd.) and stored on computer for analysis. Typically between ten and twenty intensity-versus-time profiles were averaged for each measurement at each NO_2 concentration. The concentration of C_2H_2 was on average (over the *T*-range of 288 to 800 K) 2.0×10^{14} cm^{-3} which, according to our flow calibrations, was reproducible to within $\pm3\%$ and remained stable to within $\pm2\%$ during the determination of each rate constant. The average initial concentration of C_2H in our system was calculated to be about 4×10^{11} cm^{-3}. This is based on an absorption cross section for C_2H_2 of 1.4×10^{-19} cm^{-2} at 193 nm (Ref. 54) and a quantum yield for C_2H production of near unity.[55,56] The concentration of the reactant, $[NO_2]$, was varied between 5×10^{13} cm^{-3} and 1.5×10^{15} cm^{-3} giving rise to $I(CH^*)$ intensity profiles (see below) with decay rates ranging from 0.5×10^5 s^{-1} to 4×10^5 s^{-1}. Thus the ratio $[C_2H]/[NO_2]$ was sufficiently small in these experiments (on average $\approx5\times10^{-4}$) to ensure negligible influence of any secondary or side (radical–radical) reactions which would either consume or regenerate C_2H. The rate of C_2H removal by its reactions with NO_2 and C_2H_2 is between two and three orders of magnitude higher than the expected rate of C_2H self-reactions or of C_2H with any product radicals.

B. Monitoring C_2H

It has been shown that there exists only one fragment channel for single-photon dissociation of C_2H_2 at 193 nm: C_2H+H.[55,56] A fraction of $[C_2H]$ may however be formed in its electronically excited $A\,^2\Pi$ state.[57,58] Under our experimental conditions it is expected that the decay rate of the any $[C_2H(A\,^2\Pi)]$ initially formed will be at least 6.7×10^5 s^{-1} due to collisional quenching alone by 5 Torr of N_2: based on $k_q(A\,^2\Pi\rightarrow X\,^2\Sigma)=4\times10^{-12}$ $cm^3\,s^{-1}$ for He.[58] This decay rate is more than a factor of 2 greater than the highest decay rate measured in these experiments. It has also been suggested that some C_2H_2 may remain electronically excited following 193 nm absorption by residing in a metastable triplet state—most likely as ''unreactive'' vinylidene $H_2CC(\tilde{a}\,^3B_2)$.[59] However, in contrast to earlier studies employing end-product analysis of static samples, which inferred a high quantum yield for production of the metastable triplet species,[54] state-resolved dynamic studies, in particular predissociation reaction-time studies,[55] found no indication for formation of metastable acetylene or vinylidene. This is in agreement with a very recent collision-free H-atom quantum-yield investigation that determined an average yield of 0.94 (±0.12) C_2H produced per 193 nm photon absorbed.[56] In the present work we used a relatively low 193 nm laser fluence ($\approx1.5\times10^{16}$ photons cm^{-2} $pulse^{-1}$) to suppress possible production of other species by two-photon absorption of C_2H_2.[57]

Once generated, C_2H radicals undergo rapid reaction with the co-reactant NO_2 and its precursor, C_2H_2,

$$C_2H+NO_2\rightarrow\text{products}, \tag{R1}$$

$$C_2H+C_2H_2\rightarrow\text{products}. \tag{R2}$$

Earlier studies on C_2H reactions in this laboratory[23,24] have utilized a chemiluminescence method to follow the concentration of C_2H. It relies on the presence of a high excess concentration of O_2, thus initiating the following processes:

$$C_2H+O_2\rightarrow CH(A\,^2\Delta)+\text{products} \tag{R3a}$$

$$\rightarrow\text{other products} \tag{R3b}$$

$$CH(A\,^2\Delta)\rightarrow CH(X\,^2\Pi)+h\nu(\approx431\ \text{nm}). \tag{R4}$$

Since the rate of process (R4) is (much) greater than the total rate of loss of $[C_2H]$, the concentration of $CH(A)$, and hence the observed $CH(A\rightarrow X)$ emission intensity, $I_{obs}(t)$, at $\approx$431 nm, is proportional to the product $[C_2H][O_2]$. Thus, provided $[O_2]$ remains constant during the measured decay of $[C_2H]$, $I_{obs}(t)$ is directly proportional to $[C_2H]_t$.

For the experiments reported here however a variant of the above chemiluminescence method was used that requires no O_2 addition and which has a greater sensitivity to $[C_2H]$ thus allowing a lower $[C_2H_2]$ to be used. It relies on the same emission as the former method, $CH(A)\rightarrow CH(X)$, but here $CH(A)$ is formed in high yields by the reaction of C_2H with O atoms that arise from the simultaneous 193 nm photolysis of NO_2.

According to a recent study by Sun *et al.*,[60] photolysis at 193 nm of NO_2 has two dissociation channels,

$$NO_2+h\nu(193\ \text{nm})\rightarrow O(^3P)+NO \tag{R5a}$$

$$\rightarrow O(^1D)+NO \tag{R5b}$$

with a branching fraction of 0.55 ± 0.03 to (R5b). In the same study a room temperature rate constant for $O(^1D)+NO_2$ was determined as $(1.5\pm0.3)\times10^{-10}$ $cm^{-3}\,s^{-1}$ and the absorption cross section of NO_2 at 193 nm was estimated to be $(2.9\pm1.2)\times10^{-19}$ cm^{-2}. Under our experimental conditions, a fraction of $\approx4\times10^{-3}$ of $[NO_2]$ should thus be photolyzed. The fate and possible influence of $O(^1D)$ in our system is discussed in the next section. Suffice it to say here that $O(^1D)$ atoms were effectively quenched to $(O\,^3P)$ by collisions with N_2 on time scales much shorter than the $[C_2H]$ $(1/e)$ lifetime.

The $O(^3P)$-atoms generated by (R5a) and indirectly via (R5b) will react with C_2H yielding a high fraction of electronically excited CH,[33]

$$C_2H+O\rightarrow CH(A)+\text{products} \tag{R6a}$$

$$\rightarrow\text{other products}. \tag{R6b}$$

In the presence of $O(^3P)$ atoms and once a quasisteady state is established [effectively within 2 μs given the 0.54 μs radiative lifetime of $CH(A\,^2\Delta)$ (Ref. 61)], $I_{obs}(t)$ is propor-

tional to $[C_2H]_t[O(^3P)]_t$. However, the relatively low concentration of $O(^3P)$ atoms generated in these experiments are susceptible to a small decrease during measurement of $I_{obs}(t)$. It is therefore important to know the time dependence of $[O(^3P)]_t$ in order to determine the relative $[C_2H]_t$ from $I_{obs}(t)$. More strictly, as shown below, it is only the change in $[O(^3P)]_t$ due to reaction with NO_2 that need be known in order to derive the rate constant for NO_2+C_2H from exponential decays of $I_{obs}(t)$.

Determination of $[O(^3P)]_t$ is straightforward in the present experiments since well-established reactions with known concentrations of NO_2 and with C_2H_2 are mainly responsible for its time dependence,

$$O(^3P)+NO_2 \rightarrow NO+NO, \tag{R7}$$

$$O(^3P)+C_2H_2 \rightarrow \text{products}. \tag{R8}$$

$O(^3P)$ atoms will react with NO_2 with removal rates for the present experiments between 500 s^{-1} and 15 000 s^{-1} at 298 K and about half these values at 800 K. The rate of $O(^3P)$ removal due to reaction with 4×10^{14} $cm^{-3}\times(293/T)$ of C_2H_2 is about 50 s^{-1} at 293 K and about 800 s^{-1} at 800 K,[62] and with $\approx5\times10^{11}$ cm^{-3} of C_2H is about 50 s^{-1}.[20] As $[NO_2]$ is in large excess of $[O]_0$, $[O]_t$ is described by a single-exponential decay function. This function has a much weaker dependence on time than $[C_2H]_t$ (see below). Though the reaction C_2H+O is essential for monitoring the relative C_2H concentration [channel (R6a)], the removal of C_2H due to reaction with O atoms is negligible in these investigations. The rate constant for $C_2H+O\rightarrow$products is about 9×10^{-11} cm^3 s^{-1} (Ref. 20) and that of $NO_2+C_2H\rightarrow$products—as determined in these experiments—is 1.2×10^{-10} cm^3 s^{-1}. Thus C_2H+O contributes less than 0.3% to the observed removal of C_2H and is therefore neglected in the following analysis.

The changing concentration of C_2H with time is given by

$$-\frac{d[C_2H]_t}{dt}=k_1[NO_2][C_2H]_t+k_2[C_2H_2][C_2H]_t. \tag{1}$$

Loss of C_2H through molecular diffusion or convective flow (at rates of $\sim$1000 s^{-1}) is negligible in these experiments with minimum $[C_2H]_t$ decay rates of 5×10^4 s^{-1}.

Solving Eq. (1) gives a simple exponential form for $[C_2H]_t$,

$$[C_2H]_t=[C_2H]_0\exp(-(k_1'+k_2')t), \tag{2}$$

where $k_1'=k_1[NO_2]$ and $k_2'=k_2[C_2H_2]$.

The chemiluminescence intensity $I_{obs}(t)$ is directly proportional to the concentration of electronically excited CH radicals,

$$I_{obs}(t)=\Theta k_4[CH(A)]_{ss}(t), \tag{3}$$

here Θ is a constant representing the overall photon collection efficiency of the detection system.

The time rate of change of $CH(A)$ is described by

$$\frac{d[CH(A)]_t}{dt}=k_{6a}[C_2H]_t[O]_t-(k_4+k_{qi})[CH(A)]_t, \tag{4}$$

where the term k_{qi} represents the total pseudo-first-order rate constant for physical quenching of $CH(A)$.

After several $(1/e)$ lifetimes of $CH(A)$, or ≈2 μs, i.e., on a time scale much shorter than the removal of C_2H, $[CH(A)]$ reaches a quasi-steady-state such that $d[CH(A)]/dt=0$. Under these conditions,

$$[CH(A)]_{ss}(t)=\frac{k_{6a}}{k_4+k_{qi}}[C_2H]_t[O]_t. \tag{5}$$

Since both $[NO_2]$ and $[C_2H_2]$ are in large excess of both $[O(^3P)]$ and $[C_2H]$—and therefore constant—and since removal of $O(^3P)$ by C_2H is negligible, the time dependence of $[O(^3P)]$ should follow a simple exponential function described by

$$[O(^3P)]_t=[O(^3P)]_0\exp(-(k_7'+k_8')t), \tag{6}$$

where $k_7'=k_7[NO_2]$ and $k_8'=k_8[C_2H_2]$.

Substituting Eqs. (2) and (6) into Eq. (5) and using the relation of Eq. (3) gives

$$I_{obs}(t)=\Theta\frac{k_{6a}}{k_4+k_{qi}}[C_2H]_0[O(^3P)]_0\times\exp(-(k_1'+k_2'+k_7'+k_8')t). \tag{7}$$

Therefore the $CH(A)$ chemiluminescence intensity follows a simple exponential decay described by

$$I_{obs}(t)=A\exp(-k_{total}t), \tag{8}$$

$$k_{total}=k_2'+k_8'+k_1'+k_7'=(k_2+k_8)[C_2H_2]+(k_1+k_7)[NO_2]. \tag{9}$$

The parameters k_{total} (units s^{-1}) and A are determined by a weighted least-squares fit to $I_{obs}(t)$. Each $I_{obs}(t)$ profile is determined from raw emission data by subtraction of an emission profile taken in the absence of C_2H_2 from that taken in the presence of C_2H_2. This procedure effectively distinguishes laser scattered light and window fluorescence from the desired $CH(A)\rightarrow CH(X)$ emission.

Since k_2' and k_8' are constants for a fixed $[C_2H_2]$ the term $(k_2+k_8)[C_2H_2]$ appears only as the ordinate intercept of plots of k_{total} versus $[NO_2]$. The term k_7' is however a function of $[NO_2]$, but since k_7 is well established over the temperature range of our experiments[63–68] and since $[NO_2]$ is known from flow calibrations, it may be readily calculated. Actually, k_7' contributes only about 8% to the gradient of plots of k_{total} versus $[NO_2]$ at all temperatures [when employing the $k_7(T)$ expression of Estupinan *et al.*, $k_7(T)=4.21\times10^{-12}\exp(273/T)$ (Ref. 68)]. Thus a straight line may be fitted to plots of $(k_{total}\text{-}k_7')$ versus $[NO_2]$ and the gradients will be equal to k_1: the rate constant to be determined.

III. EXPERIMENTAL RESULTS

Our initial task was to establish whether or not the initial presence of $O(^1D)$, produced by photolysis of NO_2, could interfere with our determination of k_1. Figure 2 shows two emission profiles each of 50 μs duration and collected at 298 K under identical conditions of $[C_2H_2]=5.8\times10^{14}$ cm^{-3},

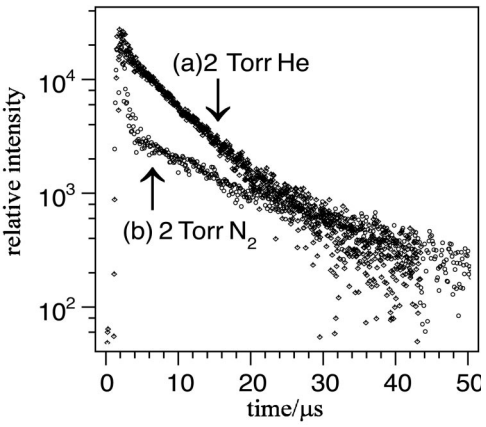

FIG. 2. Emission profiles from the center of the reaction chamber following photolysis of C_2H_2 and NO_2 in the presence excess He (plot a, diamonds) and N_2 (plot b, circles) both at a total pressure of 2 Torr. Apart from the different buffer gases the profiles were recorded under identical conditions of temperature, pressure, $[C_2H_2]$ $(t=0)$, $[NO_2]$ $(t=0)$ and 193 nm photolysis energy. The initial intensity and gradient difference between the two plots is attributed to the additional reactions, $C_2H+O(^1D)\rightarrow CH(A)+CO$ and $O(^1D)+C_2H_2\rightarrow$products, respectively in plot (a).

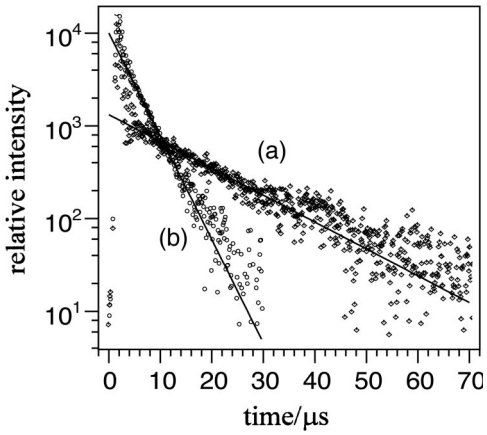

FIG. 3. Typical emission profiles, $I_{obs}(t)$, from the center of the reaction chamber following pulsed 193 nm photolysis of C_2H_2 and NO_2 in the presence of N_2 at a total pressure of 5 Torr and at a temperature of 293 K. Profile (a, diamonds): $[NO_2]=8.7\times10^{13}$ cm^{-3}. Profile (b, circles): $[NO_2]=1.1\times10^{15}$ cm^{-3}.

$[NO_2]=1.4\times10^{14}$ cm^{-3}, and at 2 Torr total pressure but in the presence of difference bath gases, He (plot a) and N_2 (plot b). Since the rate constant for quenching of $O(^1D)$ by He is less than 3×10^{-13} cm^3 s^{-1} and that for N_2 is 1.8×10^{-11} cm^3 s^{-1},[69] $O(^1D)$ will have a $(1/e)$ lifetime in these experiments with a lower limit of 51 and 0.8 μs, respectively, due to these processes. Thus any influence of $O(^1D)$ on the observed emission intensity should be revealed in the difference between profiles (a) and (b).

The most obvious difference is that the initial emission intensity [i.e., the extrapolated long-time intensity to $t=0$ neglecting that of the first 5 μs, which is due to spontaneous emission from $CH(A)$ produced initially by two-photon absorption of C_2H_2 at 193 nm] is a factor of 5 greater for the He experiment than for the N_2 experiment. This intensity difference is attributable to the presence of an additional chemiluminescence reaction, viz., $O(^1D)+C_2H\rightarrow CH(A)+CO$. Further, the rate constant for this reaction channel should be about four times greater than that for the reaction $O(^3P)+C_2H\rightarrow CH(A)+CO$ [4.5×10^{-12} cm^3 s^{-1} (Ref. 34)] if one assumes the $O(^3P)/(O\,^1D)$ branching fraction in the 193 nm photolysis of NO_2 derived by Sun *et al.*[60] This implies a large rate constant for $O(^1D)+C_2H\rightarrow CH(A)+CO$ of about 2×10^{-11} cm^3 s^{-1}—although this derivation neglects the possibility that some $O(^1D)$ or $O(^3P)$ reactions occurs with vibrationally excited C_2H. The second obvious difference between the two plots is the rate of decay of $I_{obs}(t)$. In He, this rate of decay is a factor of 2 greater. Since we have found, in a separate experiment, that the *actual increase* in decay rate of $I_{obs}(t)$ with additional NO_2 was similar for the He and N_2 experiments, we attribute the difference in slopes here mainly to fast $O(^1D)$ removal by reaction with C_2H_2. We also derive a rate constant for this reaction of about 1.3×10^{-10} cm^3 s^{-1}, similar to that of $C_2H+C_2H_2$.[23] Again, the possible influence of vibrationally excited C_2H in the He measurements is not considered here.

Thus it is clear from these measurements that, for $t\geqslant5$ μs, 2 Torr N_2 is sufficient to ensure no additional emission due to the initial presence of $O(^1D)$. Further, the very large excess of the sum $[C_2H_2]+[NO_2]$ over photolysis products ensures that there are no additional secondary or side reactions that may remove or regenerate C_2H or $O(^3P)$ sufficiently to cause a perturbation to the observed decay profiles.

Figure 3 shows two examples of $CH(A)$ emission profiles, $I_{obs}(t)$, which, as explained above, very closely represent $[C_2H]_t$. Emission profile (a) is taken under conditions of relatively low $[NO_2]$. The time dependence is therefore mainly due to reaction (2). Emission (b) is recorded in the presence of higher $[NO_2]$. A weighted least-squares fit (solid line) of each profile to Eq. (8), yields k_{total}. For $t\geqslant5$ μs, both $I_{obs}(t)$ profiles exhibit the expected simple exponential function over about two orders of magnitude. The somewhat greater emission intensity at short times of profile (b) simply reflects the increased photolytic production of $[O(^3P)]$ due to higher $[NO_2]$.

Derived k_{total} data for each $[NO_2]$ minus (the calculated) k_7' is plotted as a function of $[NO_2]$ in Fig. 4 for all temperatures covered. A linear fit to the data gives k_1 as the slope and $(k_2+k_8)[C_2H_2]$ as the intercept. As shown in Table I, the magnitude of the intercept for each temperature is in good agreement with the calculated product $(k_2+k_8)\times[C_2H_2]$, where k_2 has a T-independent value of 1.3×10^{-10}cm^3 s^{-1},[23] $k_8(T)=1.2\times10^{-17}T^{2.09}\exp(-786\text{ K}/T)$ cm^3 s^{-1} (Ref. 62) and $[C_2H_2]$ varies with T according to 4×10^{14} cm$^{-3}\times293\text{ K}/T$. Even at the highest temperature, the term $k_8[C_2H_2]$ contributes less than 5% (at 800 K) to the intercept.

The derived k_1 values of all measurement sets, also listed in Table I, show that the title reaction, (1), has a large rate coefficient of 1.17×10^{-10} cm^3 s^{-1} at 293 K that decreases slightly with increasing temperature as depicted also in the Arrhenius plot of Fig. 5. Also included both in Table I and in the Arrhenius plot of Fig. 5 are the results of 293 K measurements taken at 2 and 11 Torr total pressure (N_2).

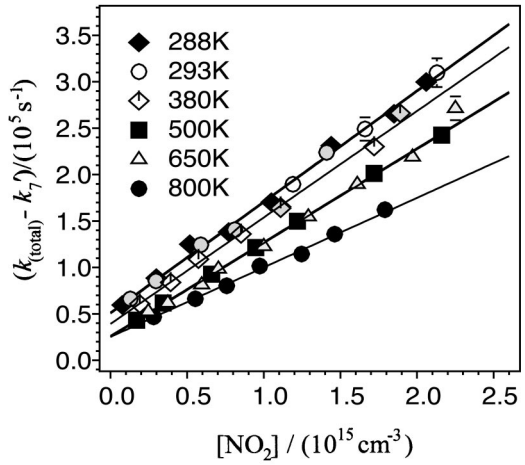

FIG. 4. Pseudo-first-order removal rate of C_2H as a function of $[NO_2]$ at several temperatures. The removal rate of C_2H is the rate of decay of the observed emission intensity minus $k_7[NO_2]$ that represents the removal rate of $[O(^3P)]$.

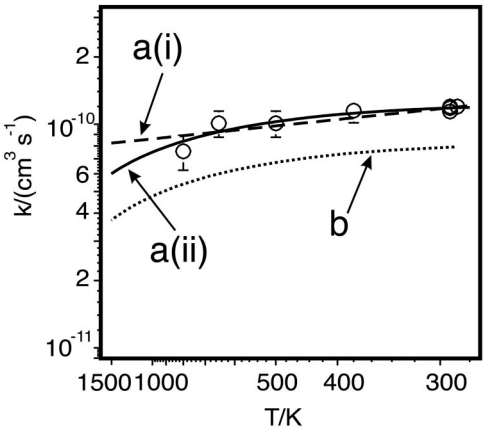

FIG. 5. (a) Arrhenius plot of the data of absolute rate constants for the reaction $C_2H+NO_2\rightarrow$products over the temperature range 288–800 K (open circles) with least-squares fits; (i) simple Arrhenius fit $\{k_1(T)=(7.6\pm1.0)\times10^{-11}\exp[(130\pm50)\ K/T]\}$, (ii) a three-parameter Arrhenius fit $\{k_1(T)=(9.7\pm1.5)\times10^{-9}T^{-0.68}\exp[(158\pm65)\ K/T]\}$. (b) Dotted curve: a best fit to rate constant data for the isoelectronic reaction $CN+NO_2\rightarrow$products, taken from Refs. 72, 73, and 74.

These results show no dependence of the overall rate constant with pressure. This finding will be expanded upon in the next sections.

The straight line in Fig. 5 represents the best simple Arrhenius fit to the data: $k_1(T)=(7.6\pm1.0)\times10^{-11}\exp[(130\pm50)\ K/T]$. The highest-temperature measurements however indicate a downward curvature in the Arrhenius plot. To allow for this, we also fitted a three-parameter Arrhenius expression to the data. This gives $k_1(T)=(9.7\pm1.5)\times10^{-9}T^{-0.68}\exp[(158\pm65)\ K/T]$. For both expressions, the stated uncertainties encompass both statistical (2σ) and likely systematic errors.

IV. QUANTUM CHEMICAL CALCULATIONS

Having established the rate constants of the C_2H+NO_2 reaction, we now attempt to identify the possible and probable product channels making use of quantum chemical calculations.

TABLE I. Measured rate constants for $C_2H+NO_2\rightarrow$products. These data also include 293 K measurements taken at 2 and 11 Torr total pressure. The experimentally determined ordinate intercepts may be compared with those expected based on $k_2[C_2H_2]+k_8[C_2H_2]$.

Temperature/ K	$k_1/(10^{-10}$ $cm^{-3}\ s^{-1})$	Ordinate intercept/s^{-1} [a,b]	$k_2[C_2H_2]+$ $k_8[C_2H_2]/s^{-1}$ [a,c]	Pressure/ Torr
288	1.20 ± 0.08	$(50\pm3)\times10^3$	53×10^3	5
293	1.14 ± 0.09	$(50\pm3)\times10^3$	52×10^3	5
293	1.20 ± 0.10			2
293	1.18 ± 0.11			11
380	1.15 ± 0.07	$(39\pm3)\times10^3$	41×10^3	5
500	1.01 ± 0.10	$(26\pm2)\times10^3$	30×10^3	5
650	1.00 ± 0.11	$(25\pm2)\times10^3$	24×10^3	5
800	0.76 ± 0.08	$(25\pm2)\times10^3$	20×10^3	5

[a]Only values for 5 Torr experiments are given.
[b]Errors are 2σ.
[c]Calculations based on $[C_2H_2]=4\times10^{14}\ cm^{-3}\times293\ K/T$, a k_2 of $1.3\times10^{-10}\ cm^3\ s^{-1}$ (Ref. 23) and a k_8 of $1.2\times10^{-17}\ T^{2.09}\times\exp(-786\ K/T)\ cm^3\ s^{-1}$ (Ref. 62).

All calculations were performed using the GAUSSIAN 98 suite of programs.[70] Geometry optimizations were conducted using density functional theory (DFT) with the popular hybrid functional, B3LYP, in conjunction with the 6-311++G(d,p) basis set. Electronic energies of the B3LYP-optimized geometries were refined using a larger basis set, 6-311++G($3df,2p$), and coupled-cluster theory with all single and double excitations plus perturbative corrections for triple substitutions, CCSD(T)/6-311++G(d,p). Harmonic vibrational wavenumbers were calculated at both Hartree Fock (HF) and B3LYP levels to characterize the stationary points as equilibrium or transition structures. The zero-point energies (ZPE) were derived from B3LYP frequencies and scaled down by the standard factor of 0.97. In the CCSD(T) calculations, the core orbitals were kept frozen. Intrinsic reaction coordinate (IRC) calculations were also performed to confirm the intermediates connected to the transition structures.

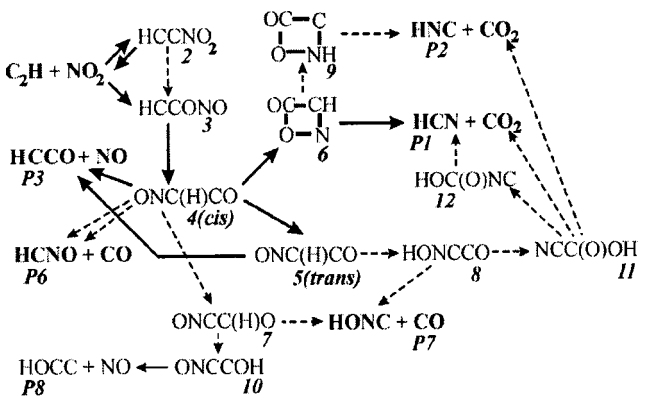

Scheme 1. A summary of the reaction paths available to the C_2H+NO_2 reaction with the exception of some minor paths leading from structure **11**. The solid arrows show the likely dominant paths. These paths lead to the product sets HCCO+NO and HCN+CO_2, and to redissociation to reactants.

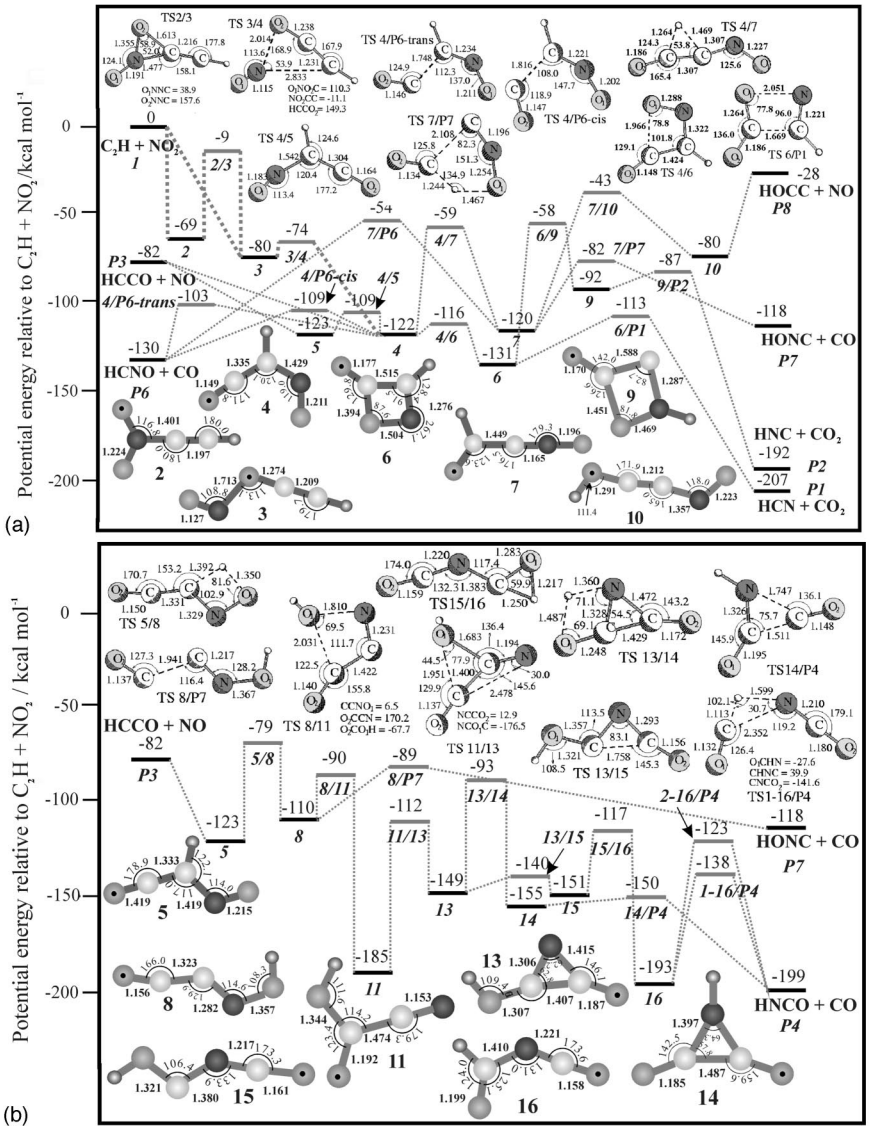

FIG. 6. The potential energy surface (PES), calculated at the CCSD(T)/6-311++G(*d*,*p*)//B3LYP/6-311++G(*d*,*p*)+ZPE level, for C_2H+NO_2. (a) The intermediates and products directly accessible from structure 4, which is always formed in this reaction. B3LYP/6-311++G(*d*,*p*)-optimized geometrical structures of the relevant intermediates are displayed at the bottom, the transition state structures are displayed at the top [TS 6/9, TS 9/P2, TS 7/10, and TS 7/P7 are displayed in Fig. 6(c)]. Bond lengths are given in angstroms and bond angles in degrees. (b) The intermediates and products directly accessible from structure 5. (c) The intermediates and products directly accessible from structure 11.

The important reaction paths (together with some minor ones) investigated in this study are shown in Scheme 1.The important paths (see Sec. VI) are shown with solid lines. For the sake of brevity some minor paths leading from structure **11** have been omitted from Scheme 1 but may be ascertained from Figs. 6(b) and 6(c). We have identified seventeen isomers, which are both open-chain and cyclic structures. The connections between them and to products are described by 32 transition structures (TS). These are all displayed in Figs. 6(a), 6(b), and 6(c) together with their associated potential energies and connections, showing all eighteen reaction pathways identified. In Figs. 6(a)–6(c) and Scheme 1 the various isomers of the $[C_2,H,N,O_2]$ system are labeled from **2** to **18**, the product sets are labeled as follows: **P1**=(HCN+CO_2), **P2**=(HNC+CO_2), **P3**=(NO+HCCO), **P4**=(CO+HNCO), **P5**=(CO+HOCN), **P6**=(CO+HCNO), and **P7**=(CO+HONC). In Figs. 6(a)–6(c) bond lengths have units of angstroms and bond angles are represented in degrees, **i/j** stands for a transition structure connecting the equilibrium structures **i** and **j**, a number in front of **TS i/j** is added if a distinction need be made between transition states connecting the same **i/j** products. The relative energies of the stationary points on the $[C_2,H,N,O_2]$ PES, which are obtained using three distinct methods, are listed in Table II. In general, the B3LYP values are comparable to those derived from the CCSD(T) method. In the following discussion, unless otherwise stated, the energies refer to those obtained from CCSD(T)/6-311++G(*d*,*p*)+ZPE.

V. QUANTUM CHEMICAL CALCULATION RESULTS

Although the C_2H+NO_2 reactive system is complex, an important simplifying feature is that all channels connecting

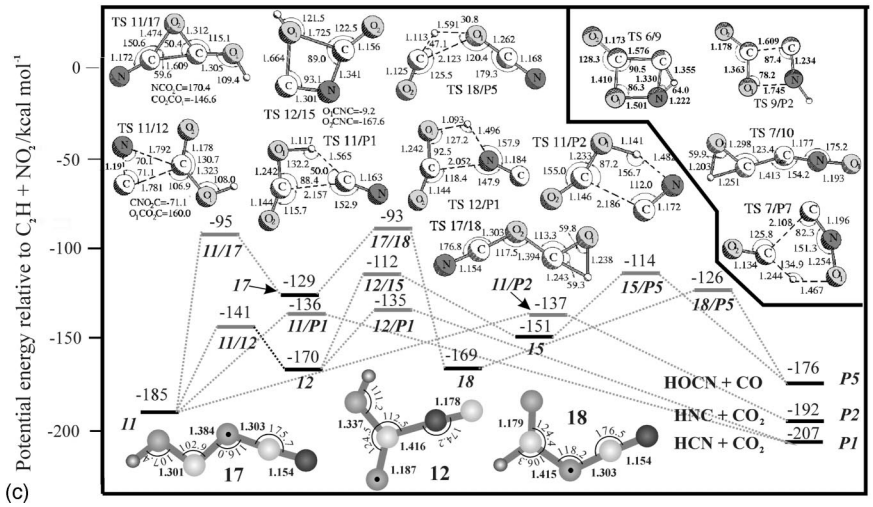

FIG. 6. (*Continued.*)

C_2H+NO_2 to products pass through intermediate **4**, *cis* nitrosoketene, which lies 122 kcal mol^{-1} below the reactants. The paths leading to **4** are shown with *thick* dashed lines in Fig. 6(a). Thus, excepting for the chance of redissociation of **2** to C_2H+NO_2 (discussed later), the distribution of the various product channels depends upon the fate of the highly excited *cis* nitrosoketene intermediate **4**. This has already been the subject of detailed RRKM-master equation analyses by Vereecken *et al.*[44] and Tokmakov *et al.*[76] in the context of the HCCO+NO reaction system, which is common to the present system at energies of 82 kcal mol^{-1} below C_2H+NO_2. However, in the HCCO+NO reaction, the *cis* nitrosoketene intermediate is formed with that much less internal energy.

Before further discussion of the likely product distribution we briefly give a description of the various product pathways. To simplify and shorten the description below we refer to the processes following the paths C_2H+NO_2, **1**→**2**→**2/3**→**3**→**3/4**→**4** or C_2H+NO_2, **1**→**3**→**3/4**→**4** as common pathways (or **CPs**) since every product channel of C_2H+NO_2 begins with either of these paths.

A. Formation of HCN+CO$_2$, P1

Three pathways terminate at $HCN+CO_2$, the most stable products. The first path contains the lowest barrier heights of the entire energy surface [Fig. 6(a)]. Proceeding from the *cis* nitrosoketene intermediate (**4**), two rearrangements have been identified. Isomer **4** has an appropriate nuclear configuration for a 1,4 electrocyclization via **TS 4/6**, which has a barrier of 6 kcal mol^{-1}. Thus, **4** leads to the four-membered ring **6** (−131 kcal mol^{-1}). Intermediate **6** can subsequently undergo a concerted cycloreversion, over a barrier of 18 kcal mol^{-1} (**TS 6/P1**), yielding **P1**.

The second path involves a transformation from **4** to **5**. Intermediate **5** is a rotamer of **4**, which is accessible by an out-of-plane N–O rotation over a small but significant (see later) barrier.[44] Structure **8** can be formed by a 1,4 hydrogen migration from **5**. **TS 8/11** (−90 kcal mol^{-1}), is the transition structure for a 1,3 hydroxyl migration connecting minima **8** and **11** with barriers of 20 and 95 kcal mol^{-1} for forward and reverse directions, respectively. The low-lying isomer **11** subsequently provides the last step for this path by undergoing a concerted 1,3-H migration and breaking of the C–C bond yielding **P1**, $HCN+CO_2$.

The final path to **P1** occurs via **TS 11/12**, which describes an exchange of the C and N atoms by an in-plane rotation yielding **12**. From **12**, C–N bond rupture together with an O-to-N H migration gives **P1**,

CPs→[**4/6**→**6**→**6/P1**]→**P1** (Path 1 P1)

CPs→[**4/5**→**5**→**5/8**→**8**→**8/11**→**11**→**11/P1**]→**P1**

(Path 2 P1)

CPs→[**4/5**→**5**→**5/8**→**8**→**8/11**→**11**→**11/12**→**12**

→**12/P1**]→**P1** (Path 3 P1).

The sections of the paths (above) enclosed with square brackets indicate the differences between paths leading to the same products. This notation will be used throughout.

B. Formation of HNC+CO$_2$, P2

The production of **P2** may occur by two pathways. One pathway ends by breaking the C–C bond of structure **11** accompanying a 1,4-hydrogen migration via **TS 11/P2** (−137 kcal mol^{-1}). The other path involves formation of a four-membered ring, **9**, from structure **6** via **TS 6/9** (−58 kcal mol^{-1}). Ring **9** subsequently undergoes a concerted [2+2] cycloreversion yielding **P2** via the **TS 9/P2** (−87 kcal mol^{-1}) with an energy barrier of only 5 kcal mol^{-1},

CPs→[**4/5**→**5**→**5/8**→**8**→**8/11**→**11**→**11/P2**]→**P2**

(Path 1 P2)

CPs→[**4/6**→**6**→**6/9**→**9**→**9/P2**]→**P2**

(Path 2 P2).

TABLE II. Relative energies (kcal/mol) of the $[C_2HNO_2]$ stationary points calculated using different methods.

System	B3LYP 6-311++G (d,p)[a]	B3LYP 6-311++G $(3df,2p)$[a]	CCSD(T) 6-311++G (d,p)[a]
1 (C_2H+NO_2)	0	0	0
2	−72	−73	−69
3	−84	−84	−80
4	−126	−126	−122
5	−127	−127	−123
6	−129	−130	−131
7	−126	−127	−120
8	−115	−115	−110
9	−90	−91	−92
10	−83	−84	−80
11	−183	−184	−185
12	−168	−169	−170
13	−150	−151	−149
14	−159	−159	−155
15	−155	−155	−151
16	−197	−197	−193
17	−126	−126	−129
18	−168	−168	−169
P1 (CO_2+HCN)	−204	−204	−207
P2 (CO_2+HNC)	−190	−190	−192
P3 (NO+HCCO)	−84	−84	−82
P4 (CO+HNCO)	−197	−197	−199
P5 (CO+HOCN)	−168	−168	−176
P6 (CO+HCNO)	−128	−129	−130
P7 (CO+HONC)	−109	−110	−118
P8 (NO+HOCC)	−27	−27	−28
TS 2/3	−12	−13	−9
TS 3/4	−78	−78	−74
TS 4/5	−110	−110	−109
TS 4/P6-*trans*	−103	−103	−103
TS 4/P6-*cis*	−110	−110	−109
TS 4/6	−118	−119	−114
TS 4/7	−69	−70	−59
TS5/8	−85	−85	−79
TS 6/P1	−114	−114	−113
TS6/9	−56	−57	−58
TS 7/P6	−68	−69	−54
TS 7/P7	−81	−82	−82
TS7/10	−51	−52	−43
TS 8/P7	−87	−87	−89
TS 8/11	−90	−89	−90
TS 9/P2	−88	−88	−87
TS 11/P1	−134	−134	−136
TS 11/P2	−136	−136	−137
TS 11/12	−137	−137	−141
TS 11/13	−115	−115	−112
TS 12/P1	−134	−134	−135
TS 12/15	−115	−116	−116
TS 13/14	−96	−98	−93
TS 13/15	−141	−142	−140
TS 14/P4	−153	−153	−150
TS 15/P5	−114	−115	−114
TS 15/16	−122	−122	−117
TS 1-16/P4	−144	−144	−138
TS 2-16/P4	−125	−125	−123
TS 11/17	−94	−95	−95
TS 17/18	−91	−92	−93
TS 18/P5	−129	−129	−126

[a]Using B3LYP/6-311++G(d,p) optimized geometries. All values are corrected for ZPEs obtained from B3LYP/6-311++G(d,p) harmonic frequencies and scaled down by 0.97.

C. Formation of HCCO+NO, P3

Scheme 1 reveals that NO+HCCO formation could occur by passage through (at least) either two, three or four isomers, depending upon the entrance channel traversed, in which the system initially passes through either the nitroacetylene **2** or the ethynylnitrite **3** isomer. We have made extensive attempts to locate a one-step transition structure directly connecting isomer **3** and HCCO+NO products, but there appears to be no such connection that lies low enough to be of any relevance. This can be readily rationalized by recognizing that breaking of the N–O(–C) bond of **3** actually leads to an HCCO structure with the unpaired electron on the O-atom. Such an HCCȮ state corresponds to linear, electronically-excited HCCO($\tilde{B}\,^2\Pi$) (H–C≡C–Ȯ) and not to its ground electronic state. The *B* state of HCCO lies about 95 kcal mol^{-1} higher[71] than the HCCO($\tilde{X}\,^2A''$) ground state and is thus not accessible by C_2H+NO_2. The only product path available to **3** then is a 1,3-NO migration over a low-lying **TS 3/4** leading to *cis* nitrosoketene. From either **4** or **5** a simple dissociation of the C–N bond leads to HCCO +NO,

CPs→**P3** (Path 1 P3)

CPs→[**4/5**→**5**]→**P3** (Path 2 P3).

D. Formation of HNCO+CO, P4

These products lie 69 kcal mol^{-1} below HCNO+CO. Their formation involves traversal of at least seven transition states. There are three pathways, namely,

CPs→**4/5**→**5**→**5/8**→**8**→**8/11**→**11**→**11/13**→**13**
→[**13/14**→**14**→**14/P4**]→**P4** (Path 1 P4)

CPs→**4/5**→**5**→**5/8**→**8**→**8/11**→**11**→**11/13**→**13**
→[**13/15**→**15**→**15/16**→**16**→**1-16/P4**]
→**P4** (Path 2 P4)

CPs→**4/5**→**5**→**5/8**→**8**→**8/11**→**11**→**11/13**→**13**
→[**13/15**→**15**→**15/16**→**16**→**2-16/P4**]
→**P4** (Path 3 P4).

These three paths diverge only after isomer **13**. All processes up to minimum **11** have already been discussed, thus we proceed from there. Isomer **11** has to overcome the **TS 11/13** (−112 kcal mol^{-1}) which describes a 1,2-OH migration leading to isomer **13** (−149 kcal mol^{-1}). From here two options that lead to **P4** are available: a 1,4-H migration via the high-lying **TS 13/14** (−93 kcal mol^{-1}) to **14** or C–C bond rupture to open the three-membered ring via **TS 13/15** (−140 kcal mol^{-1}) to give the linear **15**. The first path proceeds directly from **14** via **TS 14/P4** (−150 kcal mol^{-1}) to **P4** which involves a breaking of both the C–C and C–N bonds to eliminate CO.

Isomer **15** may proceed by a 1,2 H migration to **16**. There exists from here two paths directly connecting to **P4**. The two transition structured involved **TS 1-16/P4** (−138

kcal mol^{-1}) and **TS 2-16/P4** (-123 kcal mol^{-1}) describe the progress of a simultaneous 1,2-H migration and a C–N bond cleavage. They differ in their orientation of CO and in the position of the H-atom.

E. Formation of HOCN+CO, P5

These products lie at -176 kcal mol^{-1}. There are two pathways to these products, which deviate only after isomer **11**. There final step is a C–N bond cleavage of isomer **15** via **TS 15/P5** (-114 kcal mol^{-1}) and a C–O bond cleavage of **18** accompanied by a C-to-O migration of the H atom (**TS 18/P5**),

CPs→**4/5**→**5**→**5/8**→**8**→**8/11**→**11**→[**11/12**→**12**→**12/15**→**15**→**15/P5**]→**P5** (Path 1 P5)

CPs→**4/5**→**5**→**5/8**→**8**→**8/11**→**11**→[**11/17**→**17**→**17/18**→**18**→**18/P5**]→**P5** (Path 2 P5).

F. Formation of HCNO+CO, P6

There are three relatively simple and distinct pathways. The first two originate from minimum **4** by C–C bond rupture described by two transition states **TS 4/P6**-*cis* (-109 kcal mol^{-1}) and **TS 4/P6**-*trans* (-103 kcal mol^{-1}), which are distinguished by the different orientations of CO [Fig. 6(a)]. The third pathway involves more steps and a passage over the relatively high **TS 4/7** forming **7** before passing over the even higher **TS 7/P6** to products, which involves a concerted 1,2-H migration and rupture of the C–C bond,

CPs→[**4/P6**-*cis*]→**P6** (Path 1 P6)

CPs→[**4/P6**-*trans*]→**P6** (Path 2 P6)

CPs→[**4/7**→**7**→**7/P6**]→**P6** (Path 3 P6).

G. Formation of HONC+CO, P7

These products may be formed from **8** by breaking the C–C bond, via the **TS 8/P7** (-89 kcal mol^{-1}). Another pathway starts from **4**, in which the 1,2 hydrogen migration requires much energy to overcome **TS 4/7** (-59 kcal mol^{-1}) to yield the isomer **7**. Structure **7** may undergo a 1,4-H migration at the same time as breaking the C–C bond to form the **P7** via **TS 7/P7**,

CPs→[**4/5**→**5**→**5/8**→**8**→**8/P7**]→**P7** (Path 1 P7)

CPs→[**4/7**→**7**→**7/P7**]→**P7** (Path 2 P7).

H. Formation of HOCC+NO, P8

These are the least stable products, lying only -28 kcal mol^{-1} below the reactants. Through a 1,2-H migration isomer **7** transforms to isomer **10** via **TS 7/10** (-43 kcal mol^{-1}). The product channel **P8** is formed from isomer **10** by simple bond cleavage without a transition state. This is the highest lying product pathway that is accessible to the C_2H+NO_2 reaction,

CPs→**4/7**→**7**→**7/10**→**10**→**P8** (Path 1 P8).

VI. DISCUSSION

As, from a theoretical point of view, a three-parameter Arrhenius expression is generally expected to provide better fits, this form of expression appears to be better suited to extrapolate our data to higher temperatures. Still, for $T \geqslant 1500$ K, extrapolations should be done with caution, as the precise form of the T-dependence is not known. At $T = 1500$ K, an error of some 25% can be expected. Anyhow, for temperatures above 1500 K, NO_2 becomes less important in hydrocarbon combustion systems due to reactions such as $NO_2+H \rightarrow NO+OH$.

As far as the authors are aware, ours are the first rate constant determinations for the C_2H+NO_2 reaction. Rate constant values for the isoelectronic reaction $CN+NO_2$ have however been published[72–74] and the best modified Arrhenius fit through the available data is displayed in Fig. 5 along with the present results for C_2H+NO_2. Both reactions have rate coefficients with a negative temperature dependence—not at all unusual for radical–radical reactions. This is the result of (i) a loose variational entrance transition state, combined with (ii) a lower-lying but tight transition state from the initial intermediate to fragmentation or isomerisation products. This leads to (i) a decreased rate coefficient of the initial reactant association step with increasing temperature, due to the entrance channel variational TS becoming tighter, and (ii) to an increased preference with increasing temperature for redissociation to reactants over product formation. Which of the two effects dominates depends on the particular case. Similar negative temperature dependencies have also been observed for other reactions closely related to C_2H+NO_2, namely NCO+NO (Ref. 75) and HCCO+NO.[45,76]

Whilst it is difficult to predict the importance of the C_2H+NO_2 reaction in reburning environments without detailed kinetic modeling and without accurate knowledge of the branching fractions for C_2H+NO_2 (see below), a crude comparison with the important reburning reaction, HCCO+NO, may still be formulated.

Accepting that below about 1500 K the NO_2/NO ratio is governed only by $NO+HO_2 \rightarrow NO_2+OH$ and $NO_2+H \rightarrow NO+OH$,[77] one can write a simplified expression for the ratio of HCN formation by the reactions C_2H+NO_2 and HCCO+NO,

$$\frac{R(\mathrm{HCN})_{\mathrm{C_2H+NO_2}}}{R(\mathrm{HCN})_{\mathrm{HCCO+NO}}} = \frac{k(T)_{\mathrm{NO+HO_2}}[\mathrm{HO_2}]}{k(T)_{\mathrm{NO_2+H}}[\mathrm{H}]} \frac{k(T)_{\mathrm{C_2H+NO_2}} B_1(T)[\mathrm{C_2H}]}{k(T)_{\mathrm{HCCO+NO}} B_2(T)[\mathrm{HCCO}]}, \quad (10)$$

where $k(T)_{X+Y}$ represent the overall rate constant for the given $X+Y$ reaction,[45,78,79] while $B_1(T)$ and $B_2(T)$ are the branching fractions to the HCN product channels for the C_2H+NO_2 and HCCO+NO reactions, respectively.[44,76]

In the above ratio, the strong T-dependence of the rate constant for the channel leading to HCN of the HCCO

+NO (Refs. 44, 76) reaction is compensated by the T-dependencies of the other $k(T)$'s, such that the factor

$$\frac{k(T)_{NO+HO_2}k(T)_{C_2H+NO_2}}{k(T)_{NO_2+H}k(T)_{HCCO+NO}B_2(T)} \tag{11}$$

has only a very weak T-dependence, ranging from 0.42 at 900 K to 0.49 at 1500 K. Thus over the typical reburning temperature range (1200–1500 K) Eq. (10) may be well approximated by

$$\frac{R(HCN)_{C_2H+NO_2}}{R(HCN)_{HCCO+NO}} = 0.46\frac{[C_2H][HO_2]B_1(T)}{[HCCO][H]}. \tag{12}$$

We also note here that at the lower end of the temperature range used for reburning, large HO_2 concentrations are generated by oxidation of the hydrocarbon fuel.[80]

As explained in the experimental section, the observed downward curvature of the Arrhenius plot for C_2H+NO_2 should be due to a combination of a loose (variational) entrance channel **TS** and redissociation of a short-lived, internally excited isomer to reactants. Redissociation cannot reasonably occur beyond intermediate **2** [see Fig. 6(a)]. This is because intermediate **3** will almost certainly traverse the low-lying and fairly loose **TS 3/4** rather than reform reactants. Once **4** is formed, the fraction of redissociation is expected to be negligibly small as there is comparatively little energetic hindrance for passage to the most likely product channels.

Redissociation from minimum **2** is however very likely. The deep well of **2** will ensure complete randomization of the internal energy over all modes. Whereas it is expected that a traversal of **TS 2/3** (lying only 9 kcal mol^{-1} below reactants) will be favored at very low-temperatures, redissociation will gradually prevail with increasing temperature as the number of accessible internal states in the very loose variational entrance **TS 1/2** eventually overwhelms those of the tight **TS 2/3**. Redissociation itself is not a sufficient explanation for the rapidly diminishing rate constant at $T > 700$ K observed for this reaction, nor for that at $T \gtrsim 900$ K predicted theoretically for the similar HCCO+NO reaction.[76] This is because both systems posses two entrance channels, one of which appears not to be subject to redissociation. Thus at very high temperatures, when dissociation from one entrance channel is complete, the likely cause for the rapid decrease in rate constant for both HCCO+NO and C_2H+NO_2 at high temperatures is the gradual tightening of the variational transition state of the entrance channel that remains operative.

As mentioned earlier, partitioning between the various product channels hinges on the fate of the *cis* nitroketene rotamer **4**. Given the large amount of internal energy of **4** (at least 122 kcal mol^{-1}) one expects rapid interchange between **4** and its *trans* counterpart **5**, as the energy barrier to the pertinent (out-of-plane) rotation is only 13 kcal mol^{-1}. However, several other possibilities exist for the transformation of **4**. A quantitative prediction of the possible fate of **4**, however, is no easy task, because the conventional statistical-rate approaches (RRKM and master equation analysis) cannot be applied here. The average internal energy of ~10 kcal mol^{-1} per vibrational mode is close to the reaction barriers that **4** faces. Thus **4** lives only for one or two vibrational periods (~10^{-13} s); too short by at least an order of magnitude for statistical redistribution of its internal energy over all its vibrational modes. Therefore only a dynamical description can reliably predict the product distribution. Such a treatment is far beyond the scope of this work, so the following discussion is necessarily limited to qualitative considerations.

In the recent detailed RRKM master equation analysis by Tokmakov *et al.*[76] of intermediate **4** as formed in the HCCO+NO reaction, where its internal energy is much lower (only $\geqslant$ 41 kcal mol^{-1}) it was calculated that **4** undergoes only minor redissociation to HCCO+NO but mainly traverses the lower-lying structures **TS 4/5**, **TS 4/6**, **TS 4/P6**-*cis* or **TS 4/P6**-*trans*, with the latter two (loose) TS's dominant. However when **4** is formed in the present system, with an internal energy of $\geqslant$122 kcal mol^{-1}, the number of states available at the (variational) bottleneck for HCCO+NO formation will completely dominate those associated with the aforementioned TS's. Therefore if the C_2H+NO_2 system would still behave statistically, HCCO+NO should be the dominant products. Any crossing of **TS 4/5** will still result in HCCO+NO as **TS 5/8** lies approximately equally high as the variational **TS 5/P3**, but is much more rigid.

The dynamics will be driven by the initially highly excited modes resulting from the large potential energy release from **1** to **4**. The initial excitation of each bond will depend on which of the **CPs** is traversed. On examination of the various bond-length and bond-angle changes in traversing each of the **CPs** it is clear that relatively little of the 122 kcal mol^{-1} internal energy of **4** will reside in the C–C stretch as its bond length suffers relatively little change. Rather, it is expected that, after both **CPs**, the C–N- and C–O-stretching, and the C–C–N- and C–N–O-bending modes will be considerably excited. This situation will favor either a crossing of **TS 4/6** forming the ring structure **6** to finally yield HCN $+CO_2$, or, alternatively, a direct C–N scission of **4** to give HCCO+NO. Formation of **P6** (HCNO+CO) from **4** is unlikely under these conditions as this requires significant initial energy in the C–C stretching mode.

The product branching fraction of this system will be influenced by increasing temperature, but *only* due the effect on redissociation from minimum **2**. Structures that reach **TS 2/3** or pass directly to **3** from C_2H+NO_2 should show a branching to products that is only marginally dependent on temperature.

By elimination then, it is unlikely, from either a dynamical or statistical view point that the reaction C_2H+NO_2 will yield either HNC+CO_2 (**P2**), HNCO+CO (**P4**), HONC +CO (**P7**) or HOCC+NO (**P8**). Formation of HCNO+CO (**P6**) also seems unlikely but, at present, cannot be entirely ruled out.

Finally, even though significant redissociation to reactants is expected to occur at higher temperatures from minimum **2** (following one of the two initial association channels), the C_2H+NO_2 reaction should exhibit no pressure dependence. This is because the lifetime of **2** is too short for any collisional energy transfer to occur at $p \leqslant 1$ bar and effect the steady-state energy distribution; hence the ratio of rates

(**2**→reactants)/(**2**→**3**) at a given temperature will not be influenced by pressure. The second association channel (that leading from reactants directly to **3**) will not exhibit redissociation. Hence the rate for this channel is controlled by the rate of initial association (to **3**). These observations are supported by our experiments that show no pressure dependence of the rate constant between 2 and 11 Torr N_2. We also expect that this reaction shows no pressure-dependence until pressures much greater than 1 bar.

VII. CONCLUSIONS

The absolute rate coefficient for the reaction $C_2H + NO_2$ has been measured for the first time. The experimental temperature range covered allows reliable extrapolations of the rate coefficient to temperatures up to 1500 K. As is typical of many radical–radical reactions, the rate constant for the $C_2H + NO_2$ reaction decreases with increasing temperature and also exhibits a downward curvature. This temperature dependence is attributed to (i) an increased redissociation to reactants of one of the two initially formed adducts with increasing temperature and (ii) a tightening of the entrance channel transition states with increasing temperature.

Because of its high rate constant, the title reaction is expected to participate in NO_x flame-chemistry at temperatures below 1500 K. The likely product channels, $HCN + CO_2$ and $HCCO + NO$, which are based on our qualitative dynamical considerations, also make $C_2H + NO_2$ a potentially effective NO_x reburning reaction at low temperatures (below 1500 K), although its impact will be less than the $HCCO + NO$ reaction. A detailed experimental study of the temperature dependence of the product distribution of $C_2H + NO_2$ would be an aid to dynamical theories of chemical reactions.

ACKNOWLEDGMENTS

The authors are indebted to the Fund for Scientific Research (FWO-Vlaanderen), the KULeuven Research Council (GOA-program, and doctoral fellowship) for continuing financial support.

[1] K. D. Tucker, M. L. Kutner, and P. Thaddeus, J. Astrophys. Astron. **193**, L115 (1974).
[2] W. M. Jackson, Y. H. Bao, and R. S. Urdahl, J. Geophys. Res. [Planets] **96**, 17569 (1991).
[3] T. I. Hasegawa and S. Kwok, Astrophys. J. **562**, 824 (2001).
[4] A. J. Markwick, M. Ilgner, T. J. Millar, and T. Henning, Astron. Astrophys. **385**, 632 (2002).
[5] D. F. Strobel, Planet. Space Sci. **30**, 839 (1982).
[6] M. Allen, Y. L. Yung, and G. R. Gladstone, Icarus **100**, 527 (1992).
[7] J. O. P. Pedersen, B. J. Opansky, and S. R. Leone, J. Phys. Chem. **97**, 6822 (1993).
[8] R. J. Hoobler and S. R. Leone, J. Phys. Chem. A **103**, 1342 (1999).
[9] S. Lee and S. R. Leone, Chem. Phys. Lett. **329**, 443 (2000).
[10] F. Stahl, P. V. Schleyer, H. F. Bettinger, R. I. Kaiser, Y. T. Lee, and H. F. Schaefer, J. Chem. Phys. **114**, 3476 (2001).
[11] D. Carty, V. Le Page, I. R. Sims, and I. W. M. Smith, Chem. Phys. Lett. **344**, 310 (2001).
[12] A. B. Vakhtin, D. E. Heard, I. W. M. Smith, and S. R. Leone, Chem. Phys. Lett. **348**, 21 (2001).
[13] W. M. Shaub and S. H. Bauer, Combust. Flame **32**, 35 (1978).
[14] J. Peeters and K. Devriendt, Symp. (Int.) Combust. [Proc.] **26**, 1001 (1996).
[15] J. Peeters, Bull. Soc. Chim. Belg. **106**, 337 (1997).
[16] J. A. Miller and C. F. Melius, Combust. Flame **91**, 21 (1992).
[17] R. P. Lindstedt and G. Skevis, Symp. (Int.) Combust. [Proc.] **26**, 703 (1996).
[18] N. M. Marinov, M. J. Castaldi, C. F. Melius, and W. Tsang, Combust. Sci. Technol. **128**, 295 (1997).
[19] L. V. Moskaleva, A. M. Mebel, and M. C. Lin, Symp. (Int.) Combust. [Proc.] **26**, 521 (1996).
[20] W. Boullart, K. Devriendt, R. Borms, and J. Peeters, J. Phys. Chem. **100**, 998 (1996).
[21] M. B. Colket, Symp. (Int.) Combust. [Proc.] **21**, 851 (1986).
[22] C. S. McEnally and L. D. Pfefferle, Combust. Flame **115**, 81 (1998).
[23] H. Van Look and J. Peeters, J. Phys. Chem. **99**, 16284 (1995).
[24] J. Peeters, H. Van Look, and B. Ceursters, J. Phys. Chem. **100**, 15124 (1996).
[25] R. Sumathi, J. Peeters, and M. T. Nguyen, Chem. Phys. Lett. **287**, 109 (1998).
[26] J. Peeters, B. Ceursters, H. M. T. Nguyen, and M. T. Nguyen, J. Chem. Phys. **116**, 3700 (2002).
[27] J. Peeters, B. Ceursters, H. M. T. Nguyen, and M. T. Nguyen, J. Chem. Phys. (to be published).
[28] D. Sengupta, J. Peeters, and M. T. Nguyen, Chem. Phys. Lett. **283**, 91 (1998).
[29] B. Ceursters, H. M. T. Nguyen, J. Peeters, and M. T. Nguyen, Chem. Phys. Lett. **329**, 412 (2000).
[30] B. Ceursters, H. M. T. Nguyen, J. Peeters, and M. T. Nguyen, Chem. Phys. Lett. **262**, 243 (2000).
[31] B. Ceursters, H. M. T. Nguyen, M. T. Nguyen, J. Peeters, and L. Vereecken, Phys. Chem. Chem. Phys. **3**, 3070 (2001).
[32] K. Devriendt and J. Peeters, J. Phys. Chem. A **101**, 2546 (1997).
[33] K. Devriendt, H. Van Look, B. Ceursters, and J. Peeters, Chem. Phys. Lett. **261**, 450 (1996).
[34] A yield of 30% for $CH(A\,^2\Delta)$ production from the $C_2H + O$ reaction was given in our work (Ref. 33). This value was based on a quantum yield for C_2H production from C_2H_2 photodissociation at 193 nm of 0.25. However recent publications [A. Lauter, K. S. Lee, K. H. Jung, R. K. Vatsa, J. P. Mittal, and H. R. Volpp, Chem. Phys. Lett. **358**, 314 (2002); F. Shokoohi, T. A. Watson, H. Reisler, F. Kong, A. M. Renlund, and C. Wittig, J. Phys. Chem. **90**, 5695 (1986)] show that this quantum yield is about unity. Using this new value, our originally quoted 30% $CH(A)$ yield should be revised down to 8%. Thus the revised rate constant for $C_2H + O \rightarrow CH(A) + CO$ is reduced from $(1.8 \pm 0.7) \times 10^{-11}\,cm^3\,s^{-1}$ to $(4.5 \pm 1.8) \times 10^{-12}\,cm^3\,s^{-1}$.
[35] R. K. Lyon, Int. J. Chem. Kinet. **8**, 315 (1976).
[36] L. J. Muzio, J. K. Arand, and D. P. Teixeira, Symp. (Int.) Combust. [Proc.] **16**, 199 (1977).
[37] R. A. Perry and D. L. Siebers, Nature (London) **324**, 657 (1986).
[38] R. D. Reed, U.S. Patent 1, **274**, 637 (1969).
[39] J. O. L. Wendt, C. V. Sterling, and M. A. Matovich, Symp. (Int.) Combust. [Proc.] **14**, 897 (1973).
[40] A. L. Myerson, Symp. (Int.) Combust. [Proc.] **15**, 1085 (1975).
[41] K. J. Hughes, A. S. Tomlin, E. Hampartsoumian, W. Nimmo, I. G. Zsély, M. Ujvári, T. Turányi, A. R. Clague, and M. J. Pilling, Combust. Flame **124**, 573 (2001).
[42] H. M. T. Nguyen, R. Sumathi, and M. T. Nguyen, J. Phys. Chem. A **103**, 5015 (1999).
[43] H. M. T. Nguyen, R. Sumathi, and M. T. Nguyen, J. Phys. Chem. A **104**, 1905 (2000).
[44] L. Vereecken, R. Sumathy, S. A. Carl, and J. Peeters, Chem. Phys. Lett. **344**, 400 (2001).
[45] S. A. Carl, Q. Sun, L. Vereecken, and J. Peeters, J. Phys. Chem. A **106**, 12242 (2002).
[46] J. Grebe and K. H. Homann, Ber. Bunsenges. Phys. Chem. **86**, 587 (1992), and references therein.
[47] P. G. Smith, J. Luque, C. Park, J. B. Jeffries, and D. R. Crosley, Combust. Flame **131**, 59 (2002), and references therein.
[48] W. Boullart, M. T. Nguyen, and J. Peeters, J. Phys. Chem. **98**, 8036 (1994).
[49] K. T. Rim and J. F. Hershberger, J. Phys. Chem. A **104**, 293 (2000).
[50] U. Eickhoff and R. Temps, Phys. Chem. Chem. Phys. **1**, 243 (1999).
[51] M. T. Nguyen, W. Boullart, and J. Peeters, J. Phys. Chem. **98**, 8030 (1994).
[52] L. Vereecken, R. Sumathi, S. A. Carl, and J. Peeters, Chem. Phys. Lett. **344**, 400 (2001).

[53] J. Peeters, J. Van Hoeymissen, S. Vanhaelemeersch, and D. Vermeylen, J. Phys. Chem. **96**, 1257 (1992).
[54] K. Seki and H. Okabe, J. Phys. Chem. **97**, 5284 (1993), and references therein.
[55] (a) D. H. Mordaunt, M. N. R. Ashford, R. N. Dixon, P. Löffler, L. Schnieder, and K.-H. Welge, J. Chem. Phys. **108**, 519 (1998); (b) N. Hashimoto, N. Yonekura, and T. Suzuki, Chem. Phys. Lett. **264**, 545 (1997).
[56] A. Lauter, K. S. Lee, K. H. Jung, R. K. Vatsa, J. P. Mittal, and H. R. Volpp, Chem. Phys. Lett. **358**, 314 (2002).
[57] A. M. Wodtke and Y. T. Lee, J. Phys. Chem. **89**, 4744 (1985).
[58] F. Shokoohi, T. A. Watson, H. Reisler, F. Kong, A. M. Renlund, and C. Wittig, J. Phys. Chem. **90**, 5695 (1986).
[59] A. H. Laufer and Y. L. Yung, J. Phys. Chem. **87**, 181 (1993), and references therein.
[60] F. Sun, G. P. Glass, and R. F. Curl, Chem. Phys. Lett. **337**, 72 (2001).
[61] J. Luque and D. R. Crosley, Appl. Phys. B: Lasers Opt. **63**, 91 (1996).
[62] J. V. Michael and A. F. Wagner, Ber. Bunsenges. Phys. Chem. **94**, 2453 (1990).
[63] P. P. Bemand, M. A. A. Clyne, and R. T. Watson, J. Chem. Soc., Faraday Trans. 2 **70**, 564 (1974).
[64] A. P. Ongstad and J. W. Birks, J. Chem. Phys. **85**, 3359 (1986).
[65] R. Geers-Muller and F. Stuhl, Chem. Phys. Lett. **135**, 263 (1987).
[66] A. P. Zuev and A. Y. Starikovskii, Khim. Fiz. **10**, 190 (1991).
[67] T. Gierczak, J. B. Burkholder, and A. R. Ravishankara, J. Phys. Chem. A **103**, 177 (1999).
[68] E. G. Estupinan, J. M. Nicovich, and P. H. Wine, J. Phys. Chem. A **105**, 9697 (2001).
[69] W. B. DeMore, D. M. Golden, R. F. Hampson, C. J. Howard, C. E. Kolb, and M. J. Molina, "Chemical kinetics and photochemical data for use in stratospheric modelling: Evaluation number 12," JPL Publication 97-4, 1997.
[70] M. J. Frisch, G. W. Trucks, H. B. Schlegel *et al.*, GAUSSIAN 98, Revision A.5, Gaussian, Inc., Pittsburgh, PA, 1998.
[71] D. H. Mordaunt, D. L. Osborn, H. Choi, R. T. Bise, and D. M. Neumark, J. Chem. Phys. **105**, 6078 (1996).
[72] N. S. Wang, D. L. Yang, and M. C. Lin, Chem. Phys. Lett. **163**, 480 (1989).
[73] J. Park and J. F. Hershberger, J. Phys. Chem. **97**, 13647 (1993).
[74] S. T. Wooldridge, J. D. Mertens, H. K. Ronald, and C. T. Bowman, Symp. (Int.) Combust. [Proc.] **25**, 983 (1994), and references therein.
[75] R. Zhu and M. C. Lin, J. Phys. Chem. **104**, 10807 (2000), and references therein.
[76] I. V. Tokmakov, L. V. Moskaleva, D. V. Paschenko, and M. C. Lin, J. Phys. Chem. A **167**, 1066 (2003).
[77] P. Dagaut, J. Luche, and M. Cathonnet, Int. J. Chem. Kinet. **32**, 365 (2000).
[78] T. Ko and A. Fonijn, J. Phys. Chem. **95**, 3984 (1991).
[79] C. J. Howard, J. Am. Chem. Soc. **102**, 6937 (1980).
[80] M. Hori, N. Matsunaga, N. Marinov, W. Pitz, and C. Westbrook, Symp. (Int.) Combust. [Proc.] **27**, 389 (1998).